

# Gluon shadowing in the Glauber-Gribov model at HERA

K. Tywoniuk<sup>\*1</sup>, I. C. Arsene<sup>1</sup>, L. Bravina<sup>1,2</sup>,  
A. B. Kaidalov<sup>3</sup> and E. Zabrodin<sup>1,2</sup>

<sup>1</sup> Department of Physics, University of Oslo  
0316 Oslo, Norway

<sup>2</sup> Institute of Nuclear Physics, Moscow State University  
RU-119899 Moscow, Russia

<sup>3</sup> Institute of Theoretical and Experimental Physics  
RU-117259 Moscow, Russia

## Abstract

We calculate shadowing using new data on the gluon density of the Pomeron recently measured with high precision at HERA. The calculations are made in a Glauber-Gribov framework and Pomeron tree-diagrams are summed up within a unitarity-conserving procedure. The total cross section of  $\gamma^*A$  interaction is then found in a parameter-free description, employing gluon diffractive and inclusive distribution functions as input. A strong shadowing effect is obtained, in good agreement with several other models. Impact parameter dependence of gluon shadowing is also presented.

*Keywords:* Gribov-Regge theory; nuclear shadowing; nuclear structure function

*PACS numbers:* 12.40.Nn, 13.60.Hb, 24.85.+p

---

<sup>\*</sup>Corresponding author: [konrad@fys.uio.no](mailto:konrad@fys.uio.no)

# 1 Introduction

Nuclear shadowing is a well-established phenomenon, which attracts attention of both experimentalists and theoreticians. It was found (see [1, 2] and references therein) that the inclusive nuclear structure function is smaller in nuclei than in a free nucleon at small values of the Bjorken variable  $x \leq 0.01$ . The nature of shadowing, emerging e.g. in deep inelastic scattering (DIS), can be well understood in terms of multiparticle scattering in the target rest frame. The incoming photon is represented as a superposition of gluons, quarks, anti-quarks and their bound states. At high bombarding energies the photon converts into  $q\bar{q}$ -pair long before the target, and its hadronic component interacts coherently with several nucleons of the target nucleus. This process leads to absorption and, therefore, to nucleon shadowing (for a review see e.g. [3]). Among the important consequences of the phenomenon is, for instance, severe reduction of particle multiplicity in heavy-ion collisions at LHC energies ( $\sqrt{s} = 5.5$  TeV), since multiple scattering is connected to diffraction [4, 5, 6]. The effect can be further decomposed onto the quark shadowing and the gluon shadowing; the latter provides largest uncertainties in the theory and is a subject of our present study.

In recent years a lot of interest has been generated about the possibility of parton saturation in the nuclear wave function at the smallest  $x$  accessible at HERA, and there is an ongoing discussion if the same effects can be observed for hadron-nucleus and nucleus-nucleus collisions at RHIC. In this paper, we will focus mostly on the low- $x$  effects mentioned above. Understanding the so-called cold nuclear effects in hadron-nucleus collisions serves also as a baseline for the correct treatment of possible final state effects in nucleus-nucleus collisions, e.g. high- $p_T$  particle suppression and heavy-flavor production at RHIC.

Our starting point is noticing that a significant change in the underlying dynamics of a hadron-nucleus collision takes place with growing energy of the incoming particles. At low energies, the total cross section is well described within the probabilistic Glauber model [7], which only takes into account elastic rescatterings of the incident hadron on the various nucleons of the target nucleus. Elastic scattering is described by Pomeron exchange. At higher energies,  $E > E_{crit} \sim m_N \mu R_A$  ( $\mu$  is a characteristic hadronic scale,  $\mu \sim 1\text{GeV}$ , and  $R_A$  is the radius of the nucleus) corresponding to a coherence length

$$l_C = \frac{1}{2 m_N x}, \quad (1)$$

the typical hadronic fluctuation length can become of the order of, or even bigger than, the nuclear radius and there will be coherent interaction of constituents of the hadron with several nucleons of the nucleus. The sum of all diagrams was calculated by Gribov [8, 9], which corrected the Glauber series by taking into account the diffractive intermediate states in the sum over subsequent rescatterings. The space-time picture analogy to the Glauber series is nevertheless lost, as the interactions with different nucleons of the nucleus occurs nearly simultaneous in time. The phenomenon of coherent multiple scattering is referred to as shadowing corrections.

An additional effect which comes into play at high energies, is the possibility of interactions between soft partons of the different nucleons in the nucleus. In the Glauber-Gribov

model this corresponds to interactions between Pomerons. These diagrams are called enhanced diagrams [10], and can also be understood as interactions between strings formed in the collision. Actually, the necessity to include such diagrams at high energies can be related to unitarization of the total cross section. There is a connection between these effects and saturation effects already mentioned earlier.

The Glauber-Gribov model is described and a unitarity-conserving procedure for finding the total cross section of  $\gamma^*$ -nucleus ( $\gamma^*A$ ) interaction, which corresponds to summing up Pomeron fan-diagrams, is presented in Sec. 2. Further we will concentrate on new and interesting data on gluon diffractive distribution function, which we will describe in Sec. 3. The results for gluon shadowing are presented in Sec. 4, and our conclusions are drawn in Sec. 5.

## 2 The Model

We consider the nucleus as a set of nucleons, in the spirit of the Glauber model. The elastic  $\gamma^*A$  scattering amplitude can then be written as the sum of diagrams shown in Fig. 1, i.e. as multiple  $\gamma^*$ -nucleon ( $\gamma^*N$ ) scattering diagrams with Pomeron exchange [4, 11]. The contribution from 1, 2... scatterings

$$\sigma_{\gamma^*A} = A\sigma_{\gamma^*N} + \sigma_{\gamma^*A}^{(2)} + \dots, \quad (2)$$

should be summed up to obtain the total cross section. In Eq. (2), the first term simply equals to the Glauber elastic contribution and subsequent terms describe multiple interactions of the incoming probe with the nucleons in the target nucleus.

The multiparticle content of subsequent diagrams in Fig. 1 is given by AGK cutting rules [12], where the intermediate states are on-shell. The cut contribution of the double rescattering diagram can be expressed in terms of diffractive deep inelastic scattering (DDIS). The usual variables for DDIS:  $Q^2, x, M^2$  and  $t$ , or  $x_P$ , are shown in Fig. 2. The variable  $\beta = \frac{Q^2}{Q^2 + M^2} = x/x_P$  plays the same role for the Pomeron as the Bjorken variable,  $x$ , for the nucleon. We assume that the amplitude of the process is purely imaginary; this is justified for a value of the Pomeron intercept close to unity [13]. The contribution from the second term in Eq. (2) to the total  $\gamma^*A$  cross section is given by [4]

$$\begin{aligned} \sigma_{\gamma^*A}^{(2)} = & -4\pi A(A-1) \times \\ & \times \int d^2b T_A^2(b) \int_{M_{min}^2}^{M_{max}^2} dM^2 \left[ \frac{d\sigma_{\gamma^*N}^D(Q^2, x_P, \beta)}{dM^2 dt} \right]_{t=0} F_A^2(t_{min}), \end{aligned} \quad (3)$$

where  $T_A(b) = \int_{-\infty}^{+\infty} dz \rho_A(\mathbf{b}, z)$  is the nuclear normalized density profile,  $\int d^2b T_A(b) = 1$ . The form factor  $F_A$  is given by

$$F_A(t_{min}) = \int d^2b J_0(\sqrt{-t_{min}}b) T_A(b), \quad (4)$$

where  $t_{min} = -m_N^2 x_P^2$ , and  $J_0(x)$  denotes the Bessel function of the first kind. Strictly speaking, Eq. (3) is valid for nuclear densities which depend separately on  $\mathbf{b}$  and  $z$ , however

we have checked that calculations with an exact expression lead to negligible corrections. Note that since Eq. (3) is obtained under very general assumption, i. e. analyticity and unitarity, it can be applied for arbitrary values of  $Q^2$  provided  $x$  is very small. We have assumed  $R_A^2 \gg R_N^2$ , so that the  $t$ -dependence of the  $\gamma^*N$  cross section has been neglected. For a deuteron, the double rescattering contribution has the following form

$$\sigma_{\gamma^*d}^{(2)} = -2 \int_{-\infty}^{t_{min}} dt \int_{M_{min}^2}^{M_{max}^2} dM^2 \frac{d\sigma_{\gamma^*N}^{\mathcal{D}}}{dM^2 dt} F_D(t), \quad (5)$$

where  $F_D(t) = \exp(at)$ , with  $a = 40 \text{ GeV}^{-2}$  [4].

In Eqs. (3) and (5),  $M_{min}^2$  corresponds to the minimal mass of the diffractively produced hadronic system,  $M_{min}^2 = 4m_\pi^2 = 0.08 \text{ GeV}^2$ , and  $M_{max}^2$  is chosen according to the condition:  $x_{\mathcal{P}} \leq x_{\mathcal{P}}^{max}$ . The choice of  $x_{\mathcal{P}}^{max}$  is governed by the fact that the model is only valid for  $x_{\mathcal{P}} \ll 1$ , i. e. a large rapidity gap is required in the experimental data. We use the standard choice for  $x_{\mathcal{P}}^{max} = 0.1$  [14]. It is convenient as it guarantees the disappearance of nuclear shadowing at  $x \sim 0.1$  as in experimental data. Coherence effects are taken into account through  $F_A(t_{min})$  in Eq. (4), which is equal to 1 at  $x \rightarrow 0$  and decreases with increasing  $x$  due to the loss of coherence for  $x > x_{crit} \sim (m_N R_A)^{-1}$ . In the numerical calculations, a 3-parameter Woods-Saxon nuclear density profile with parameters from [15] has been used.

Higher order rescatterings in Eq. (2) are model dependent. We use the Schwimmer unitarization [16] for the total  $\gamma^*A$  cross section which is obtained from a summation of fan-diagrams with triple-Pomeron interactions. It was checked in [4] that it gives results very close to other reasonable models, such as the quasi-eikonal model. The total cross section is then

$$\sigma_{\gamma^*A}^{Sch} = \sigma_{\gamma^*N} \int d^2b \frac{A T_A(b)}{1 + (A-1)f(x, Q^2)T_A(b)}, \quad (6)$$

where

$$f(x, Q^2) = \frac{4\pi}{\sigma_{\gamma^*N}} \int_{M_{min}^2}^{M_{max}^2} dM^2 \left[ \frac{d\sigma_{\gamma^*N}^{\mathcal{D}}}{dM^2 dt} \right]_{t=0} F_A^2(t_{min}). \quad (7)$$

Equation (6) does not take into account the shadowing effects of valence quarks nor anti-shadowing effects, which may play an important role for  $x \gtrsim 0.1$  [1].

Nuclear shadowing is studied in terms of the ratios of cross sections per nucleon for different nuclei, defined as

$$R(A/B) = \frac{B}{A} \frac{\sigma_{\gamma^*A}}{\sigma_{\gamma^*B}}, \quad (8)$$

as a function of  $x$ , which can in turn be expressed via structure functions of the different nuclei. The simplest case is  $B=N$ , then

$$R^{Sch}(A/N)(x) = \int d^2b \frac{T_A(b)}{1 + (A-1)f(x, Q^2)T_A(b)}. \quad (9)$$

In this framework shadowing can also be calculated at a fixed value of the impact parameter  $b$  for given values of  $\{x, Q^2\}$

$$R^{Sch}(A/N)(b) = \frac{1}{1 + (A-1)f(x, Q^2)T_A(b)}. \quad (10)$$

Thus the total  $\gamma^*A$  cross section can be calculated within the Glauber-Gribov model in a parameter-free way provided the total  $\gamma^*N$  cross section and the differential cross section for diffractive production are known.

### 3 Diffractive parton densities from HERA

The cross sections of the inclusive and diffractive processes are expressed through the nucleon structure functions, which are in turn associated with distribution functions of partons in the nucleon and in the Pomeron. In DIS the structure function of a nucleon,  $F_2(x, Q^2)$ , is related to the total cross section of  $\gamma^*N$  interaction through

$$\sigma_{\gamma^*N} = \frac{4\pi^2\alpha_{em}}{Q^2} F_2(x, Q^2) ,$$

valid at small  $x$ . Similar to the inclusive DIS case, a factorization theorem has been proven in perturbative QCD to hold for diffractive structure functions [17]. The relation between the diffractive cross section and the diffractive structure function is given by

$$\left[ \frac{d\sigma_{\gamma^*N}^D(Q^2, x_P, \beta)}{dM^2 dt} \right]_{t=0} = \frac{4\pi^2\alpha_{em} B}{Q^2 (Q^2 + M^2)} x_P F_{2D}^{(3)}(Q^2, x_P, \beta)$$

where the usual factorization has been assumed:

$$\frac{d\sigma_{\gamma^*N}^D(x, Q^2, M^2, t)}{dM^2 dt} = \left[ \frac{d\sigma_{\gamma^*N}^D(x, Q^2, M^2)}{dM^2 dt} \right]_{t=0} e^{Bt} .$$

A further assumption about the lower part of Fig. 2, the so-called Regge factorization [18], allows us to write the diffractive structure function as

$$F_{2D}^{(3)}(x_P, Q^2, \beta) = f_P(x_P) F(\beta, Q^2) . \quad (11)$$

The first factor is referred to as the ( $t$ -integrated) Pomeron flux (we will not take into account the sub-leading contributions from other reggeon trajectories), which is in turn defined as

$$f_P(x_P) = A_P \int_{t_{cut}}^{t_{min}} \frac{e^{B_0 t}}{x_P^{2\alpha_P(t)-1}} dt ,$$

where  $A_P$  is a constant that fixes the normalization of the flux, and  $t_{cut} = -1 \text{ GeV}^2$ . As usual, we assume a linear Pomeron trajectory,  $\alpha_P(t) = \alpha_P(0) + \alpha'_P t$ . The second factor in Eq. (11),  $F(\beta, Q^2)$ , is the Pomeron structure function. For the sake of simplicity, Eq. (7) can now be reduced to

$$f(x, Q^2) = 4\pi \int_x^{x_P^{max}} dx_P B(x_P) \frac{F_{2D}^{(3)}(x_P, Q^2, \beta)}{F_2(x, Q^2)} F_A^2(t_{min}) , \quad (12)$$

where  $B(x_P) = B_0 + \alpha'_P \ln \frac{1}{x_P}$ . The ratio of structure functions in the integrand can be understood as the density of partons in the Pomeron compared to the density of partons in the nucleon.

The determination of the distribution of partons in the nucleon and Pomeron cannot be carried out in pQCD, since it depends on soft processes such as confinement. The inclusive distributions are measured in DIS experiments to high accuracy and predictions of

the DGLAP evolution are in good agreement with experiment for a broad range of  $x$  and  $Q^2$  values. Yet, the experimental status of the diffractive distribution functions was, until recently, uncertain. The biggest uncertainty was related to the gluon distribution, because it is not measured directly in the experiment. Some authors therefore assumed that the shadowing from quarks and gluons are of equal strength [19, 20, 21], while others predicted that the gluon shadowing dominates [22, 23, 24].

The results of new high-precision measurements of the diffractive parton distribution functions (DPDFs) presented by the H1 Collaboration [25, 26], shed new light on the role of gluon shadowing at intermediate  $Q^2$ . The quark singlet and gluon DPDFs were fitted by a simple function

$$\beta f_i^{\mathcal{D}}(\beta, Q_0^2) = A_i \beta^{-B_i} (1 - \beta)^{C_i} \quad (13)$$

$$\beta g^{\mathcal{D}}(\beta, Q_0^2) = A_g \beta^{-B_g} (1 - \beta)^{C_g}, \quad (14)$$

where  $A_i$ ,  $B_i$  and  $C_i$  are fitting parameters, at a given  $Q_0^2 \sim 2 \text{ GeV}^2$ . In general, to ensure that the r.h.s. of Eq. (14) always disappears as  $\beta \rightarrow 1$ , it should be multiplied by  $\exp\left(\frac{-0.01}{1-x}\right)$ . QCD evolution to arbitrary  $Q^2$  was performed by the H1 group. For the quark singlet distribution, all three parameters  $\{A_q, B_q, C_q\}$  were used in the fit, while the gluon density is found to be insensitive to the  $B_g$  parameter, which is therefore set to zero. This fit is referred to as the 'FIT A'. Additionally, because of DGLAP evolution, data at  $\beta \geq 0.3$  cannot constrain the gluon density because of the large quark contribution to the  $Q^2$  evolution. This lack of sensitivity is confirmed by repeating the fit with the parameter  $C_g$  set to zero, and is further referred to as the 'FIT B'. The values of the corresponding Pomeron parameters are listed in Tab. 1. The fitted quark singlet distributions of 'FIT A' and 'FIT B' are consistent with each other.

Inclusion of diffractive di-jet production in the analysis provides a big improvement in the precision of the gluon density measurement [27], which can be further constrained by the diffractive production of charm in DIS [28]. A combined fit to DDIS data and diffractive di-jets [27] results in a curve similar to fit B (described above) yet with a slightly smaller gluon density at  $\beta > 0.5$ . For completeness, we also compare the new results with the old H1 parameterization [29] presented in 2002 (corresponding Pomeron parameters are given in Table 1).

The gluon distribution is almost a factor of 10 bigger than the quark distribution at the same  $Q^2$  for a broad region of  $\beta$  [25, 26]. Shadowing from quarks was calculated in [11] using the old H1 parameterizations, and we have checked that the new H1 data are consistent with their calculations. Furthermore, in the relevant kinematical range for hadron-nucleus and nucleus-nucleus collisions at RHIC and LHC, the gluon density dominates. In what follows, we will therefore consider structure functions of gluons in nuclei. The first term in Eq. (2) is then proportional to  $AG_N(x, Q^2)$ , while the second rescattering term is correspondingly equal to  $-A(A-1)G_N(x, Q^2) \int d^2T_A(b)^2 f(x, Q^2)$ , where

$$f(x, Q^2) = 4\pi \int_x^{x_P^{max}} dx_P B(x_P) f_P(x_P) \frac{\beta g^{\mathcal{D}}(\beta, Q^2)}{G_N(x, Q^2)} F_A^2(t_{min}). \quad (15)$$

Thus the gluon shadowing factor,  $R_g$ , is calculated according to Eq. (9) with  $f(x, Q^2)$  given by Eq. (15). The gluon distribution of the nucleon,  $G_N(x, Q^2) = xg(x, Q^2)$ , was taken from CTEQ6M parameterization [30].

The model for diffractive production by virtual photon described above is applicable for intermediate  $Q^2 > 1 - 2 \text{ GeV}^2$  [25, 26]. It is also important to keep in mind that the parameterization of H1 data leads to a violation of unitarity for  $x \rightarrow 0$  and should be modified at very low  $x$  (probably already at  $x \sim 10^{-4}$  for low  $Q^2$ ) [31]. Therefore our predictions are reliable in the region  $x > 10^{-4}$  which is relevant for RHIC and most experiments at LHC, and should be taken with care for  $x < 10^{-4}$ .

## 4 Numerical results

Gluon shadowing for deuteron and various heavy ions (Ca, Pd and Au) at  $Q^2 = 6.5 \text{ GeV}^2$  is presented in Fig. 3. We have made the calculations using two fits of the gluon diffractive distribution function, FIT A and FIT B. The gluon shadowing is very strong at small  $x$ , and disappearing at  $x = x_P^{max}$ . This is a consequence of the coherence effect in the form factor Eq. (4), and the vanishing integration domain in Eq. (12). Gluon shadowing is as low as 0.35 for the Au/nucleon ratio. In Fig. 4 shadowing in Pb is shown for different values of  $Q^2$ . We have also included the result using the 2002 H1 parameterization for  $Q^2 = 6.5 \text{ GeV}^2$ . Although the difference for the experimentally measured gluon distribution function is quite substantial, the shadowing contribution is stable, changing maximally 30% for the lowest  $x$ .

There is little change to be observed in the gluon shadowing ratio with increasing  $Q^2$ . The QCD evolution of the main term and rescattering terms are effectively treated separately in our approach, and therefore the shadowing correction has a slow, logarithmic dependence on  $Q^2$  [32]. The  $Q^2$  dependence of shadowing was studied within a similar model in [4] and good agreement with existing data was found.

A comparison of the results of our model with other predictions is presented in Fig. 5 for Pb at  $Q^2 = 5 \text{ GeV}^2$ . For all  $x \leq 10^{-1}$  our model predicts slightly stronger gluon shadowing compared to FGS [24], while models based on global fits to existing data on nuclear modifications and DGLAP evolution [33, 34] predict a modest gluon shadowing effect. The authors of [24] have made calculations in a similar framework as the presented model, using a quasi-eikonal summation of higher-order diagrams. In general, the quasi-eikonal model gives rise to a stronger shadowing effect than models including enhanced diagrams, i.e. Pomeron interactions, like the Schwimmer model, at  $x < 10^{-3}$ . This is not so clear from the figure as the authors of [24] put  $x_P^{max} = 0.03$  and include anti-shadowing for gluons. The quasi-eikonal model will, at asymptotical energies, lead to the grey disc limit.

We have also calculated the impact parameter dependence of Glauber-Gribov gluon shadowing given  $x = 10^{-3}$  and  $Q^2 = 5 \text{ GeV}^2$ , and compared it to results from [24] in both “high” and “low” gluon shadowing mode. Our model predict shadowing in agreement with the strongest FGS prediction, which is 20% lower than in the “low” gluon shadowing mode for central impact parameters. The shape seems to be compatible between the two models. We have also checked that agreement with the FGS model improves when updated H1

parameterizations are used [35].

## 5 Conclusions

Calculations of gluon shadowing in heavy-ions and deuteron have been made within the Gribov-Glauber model, which is a parameter-free framework to calculate shadowing effects in hadron-nucleus collisions at high energy. Diffractive structure functions have been parameterized using the latest NLO QCD fits from HERA experiments. Rather substantial shadowing effects are predicted for heavy nuclei at  $x < 10^{-3}$ , which is slowly changing with increasing  $Q^2$ . This will have implications for both light and heavy particle production in hadron-nucleus collisions at RHIC and LHC, where the relevant  $\{x, Q^2\}$  range is being probed.

Comparison to other models predicting strong shadowing effects at  $x < 10^{-2}$  have been performed. Calculations of Glauber-Gribov shadowing using Schwimmer summation of fan diagrams differ from other approaches within the same framework mainly due to differences in the treatment of higher order rescatterings, which is important in the low- $x$  region, and due to differences in the QCD evolution in  $\log Q^2$ . The advantages of our method is the clear treatment of these effects within a well-established framework.

The nuclear PDFs can be measured in ultra-peripheral collisions at both RHIC and LHC [36]. In the future, hopefully an electron-ion collider (eRHIC) would provide clear information about DIS on nuclei which would dramatically improve our understanding of high-energy nuclear effects such as shadowing.

## Acknowledgments

The authors would like to thank N. P. Armesto, A. Capella, V. Guzey and M. Strikman for interesting discussions, and V. Guzey for providing updated curves for the figures. This work was supported by the Norwegian Research Council (NFR) under contract No. 166727/V30, QUOTA-program, RFBF-06-02-17912, RFBF-06-02-72041-MNTI, INTAS 05-103-7515, grant of leading scientific schools 845.2006.2 and support of Federal Agency on Atomic Energy of Russia.

## References

- [1] M. Arneodo, Phys. Rep. **240** (1994) 301
- [2] D.F. Geesaman, K. Saito, and A.W. Thomas, Ann. Rev. Nucl. Part. Sci. **45** (1995) 337
- [3] N. Armesto, J. Phys. G **32** (2006) R367
- [4] A. Capella, A.B. Kaidalov, C. Merino, D. Pertermann, and J. Tran Thanh Van, Eur. Phys. J. C **5** (1998) 111
- [5] L. Frankfurt, V. Guzey, M. McDermott, and M. Strikman, JHEP **0202** (2002) 027
- [6] L. Frankfurt, M. Strikman, and C. Weiss, Ann. Rev. Nucl. Part. Sci. **55** (2005) 403



- [7] R. J. Glauber, in Lectures in Theoretical Physics, edited by W. E. Brittin and L. G. Dunham (Interscience, N. Y., 1959), Vol. 1, p. 315
- [8] V. N. Gribov, Sov. Phys. JETP **29** (1969) 483 [Zh. Eksp. Teor. Fiz. **56** (1969) 893]; Sov. Phys. JETP **30** (1970) 709 [Zh. Eksp. Teor. Fiz. **57** (1969) 1306]
- [9] V. N. Gribov, Sov. Phys. JETP **26** (1968) 414 [Zh. Eksp. Teor. Fiz. **53** (1967) 654]
- [10] A. Kaidalov, Nucl. Phys. A **525** (1991) 39c
- [11] N. Armesto, A. Capella, A. B. Kaidalov, J. López-Albacete, and C. A. Salgado, Eur. Phys. J. C **29** (2003) 531
- [12] V. A. Abramovsky, V. N. Gribov, and O. V. Kancheli, Yad. Fiz. **18** (1973) 595 [Sov. J. Nucl. Phys. **18** (1974) 308]
- [13] A. Capella, E. G. Ferreira, A. B. Kaidalov, and C. A. Salgado, Phys. Rev. D **63** (2001) 054010
- [14] A. B. Kaidalov, Phys. Rep. **50** (1979) 157
- [15] C. W. De Jager, H. De Vries, and C. De Vries, Atom. Data Nucl. Data Table **14** (1974) 479
- [16] A. Schwimmer, Nucl. Phys. B **94** (1975) 445
- [17] J. C. Collins, Phys. Rev. D **57** (1998) 2051; Erratum, *ibid.* D **61** (2001) 019902
- [18] C. Adloff et al., Z. Phys. C **76** (1997) 613
- [19] A. Capella, A. B. Kaidalov, and J. Tran Thanh Van, Heavy Ion Phys. **9** (1999) 169
- [20] M. Gyulassy and X. N. Wang, Phys. Rev. D **51** (1991) 64
- [21] K. J. Eskola, V. J. Kolhinen, and C. A. Salgado, Eur. Phys. J. C **9** (1998) 61
- [22] Z. Huang, H. J. Lu, and I. Sarcevic, Nucl. Phys A **637** (1998) 79
- [23] H. Hammon, H. Stocker, and W. Greiner, Phys. Lett. B **448** (1999) 290
- [24] L. Frankfurt, V. Guzey, and M. Strikman, Phys. Rev. D **71** (2005) 054001
- [25] A. Aktas et al., Eur. Phys. J. C **48** (2006) 715
- [26] A. Aktas et al., Eur. Phys. J. C **48** (2006) 749
- [27] M. Mozer, “Diffractive di-jets and combined fits”, talk at the 14th International Workshop on Deep Inelastic Scattering, DIS 2006, Tsukuba [H1prelim-06-016]
- [28] M. Kapishin, “Diffractive final states, dijets and charm”, talk at the 23rd International Conference on High Energy Physics, ICHEP 2006, Moscow
- [29] H1 Collaboration, “Measurement and NLO DGLAP QCD Interpretation of Diffractive Deep-Inelastic Scattering at HERA”, paper **980** submitted to the 31st International Conference on High Energy Physics, ICHEP 2002, Amsterdam [H1prelim-02-012]
- [30] J. Pumplin, D.R. Stump, J. Huston, H.L. Lai, P. Nadolsky, and W.K. Tung, JHEP **0207** (2002) 012
- [31] A. B. Kaidalov, V. A. Khoze, A. D. Martin, and M. G. Ryskin, Phys. Lett. B **567** (2003) 61

- [32] S. J. Brodsky, P. Hoyer, N. Marchal, S. Peigné, and F. Sannino, Phys. Rev. D **65** (2002) 114025
- [33] K. J. Eskola, V. J. Kolhinen, and C. A. Salgado, Eur. Phys. J C **9** (1999) 61; K. J. Eskola, V. J. Kolhinen, and P. V. Ruuskanen, Nucl. Phys. B **535** (1998) 351
- [34] M. Hirai, S. Kumano, and M. Miyama, Phys. Rev. D **64** (2001) 034003
- [35] V. Guzey, private communication
- [36] M. Strikman, R. Vogt, and S. White, Phys. Rev. Lett. **96** (2006) 082001

## List of Figures

1	The single and double scattering contribution to the total $\gamma^*N$ cross section. . . . .	12
2	DDIS kinematical variables in the infinite momentum frame. . . . .	13
3	Gluon shadowing for deuteron (dash-dotted curves) and for heavy ions: Ca (dotted curves), Pd (dashed curves), Au (solid curves). Black curves are for FIT A and grey curves are for FIT B. . . . .	14
4	Gluon shadowing for Pb for different virtualities, $Q^2$ . . . . .	15
5	Comparison of the results of the Glauber-Gribov model with FGS model [24], EKS [33] and HKM [34] parameterizations. . . . .	16
6	Impact parameter dependence of gluon shadowing in the Glauber-Gribov model, compared to the predictions of FGS [24]. . . . .	17

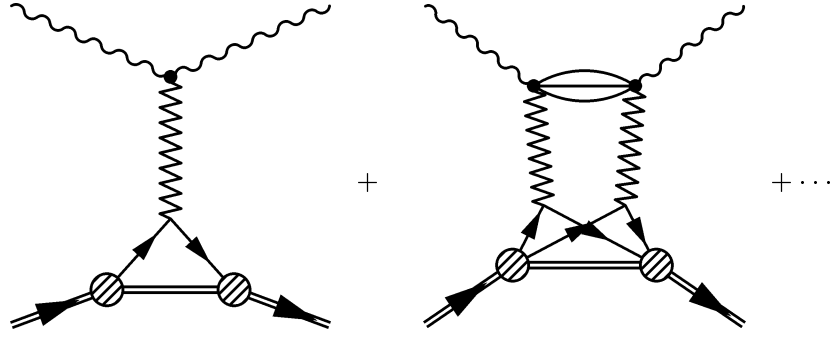


Figure 1: The single and double scattering contribution to the total  $\gamma^* N$  cross section.

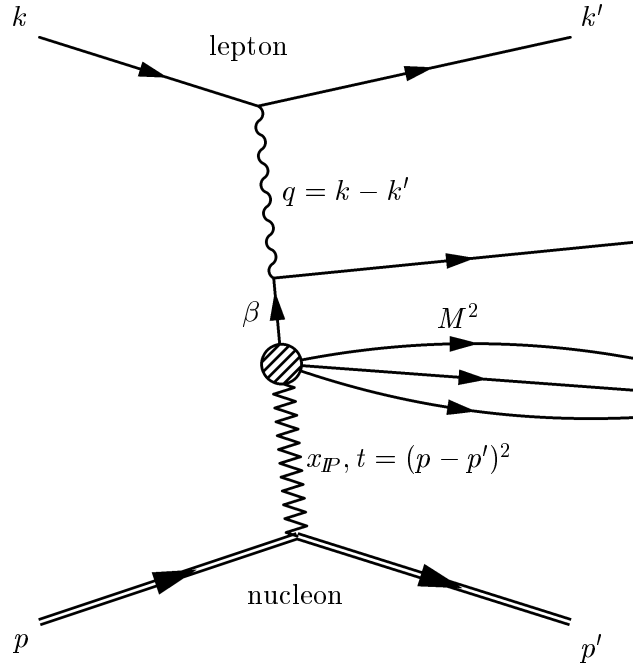


Figure 2: DDIS kinematical variables in the infinite momentum frame.

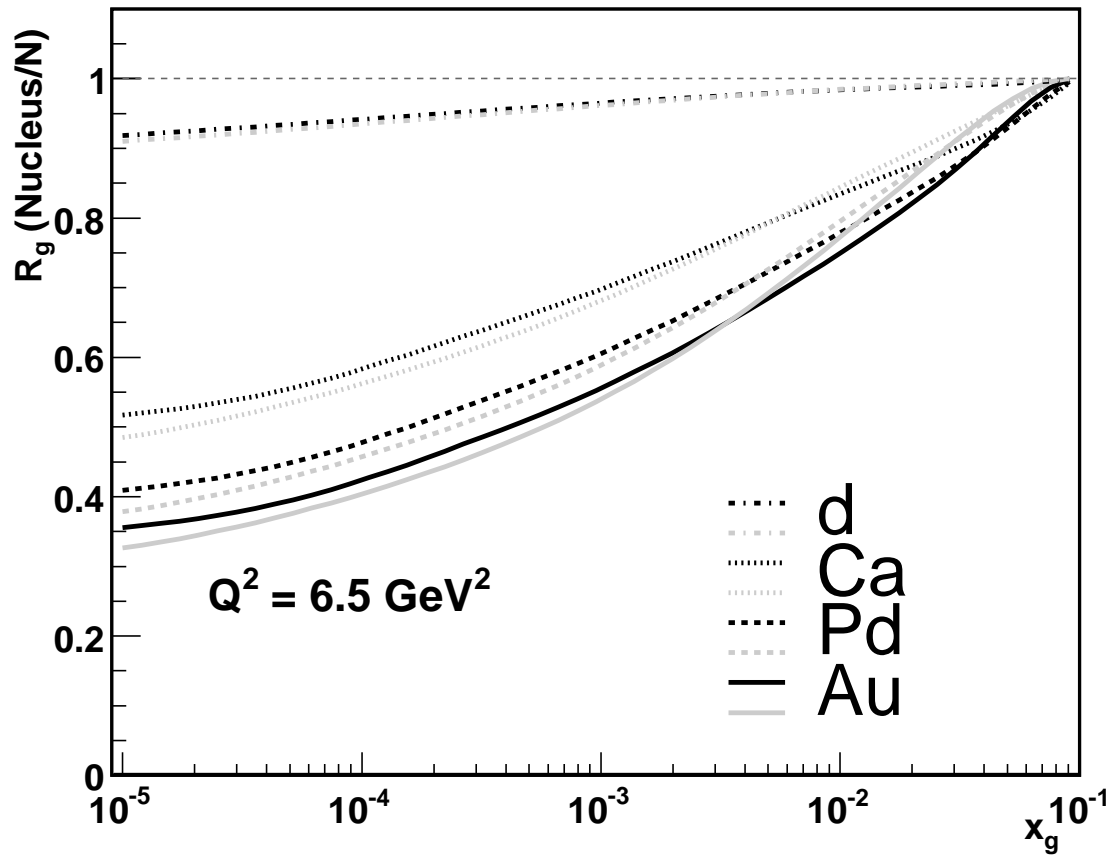


Figure 3: Gluon shadowing for deuteron (dash-dotted curves) and for heavy ions: Ca (dotted curves), Pd (dashed curves), Au (solid curves). Black curves are for FIT A and grey curves are for FIT B.

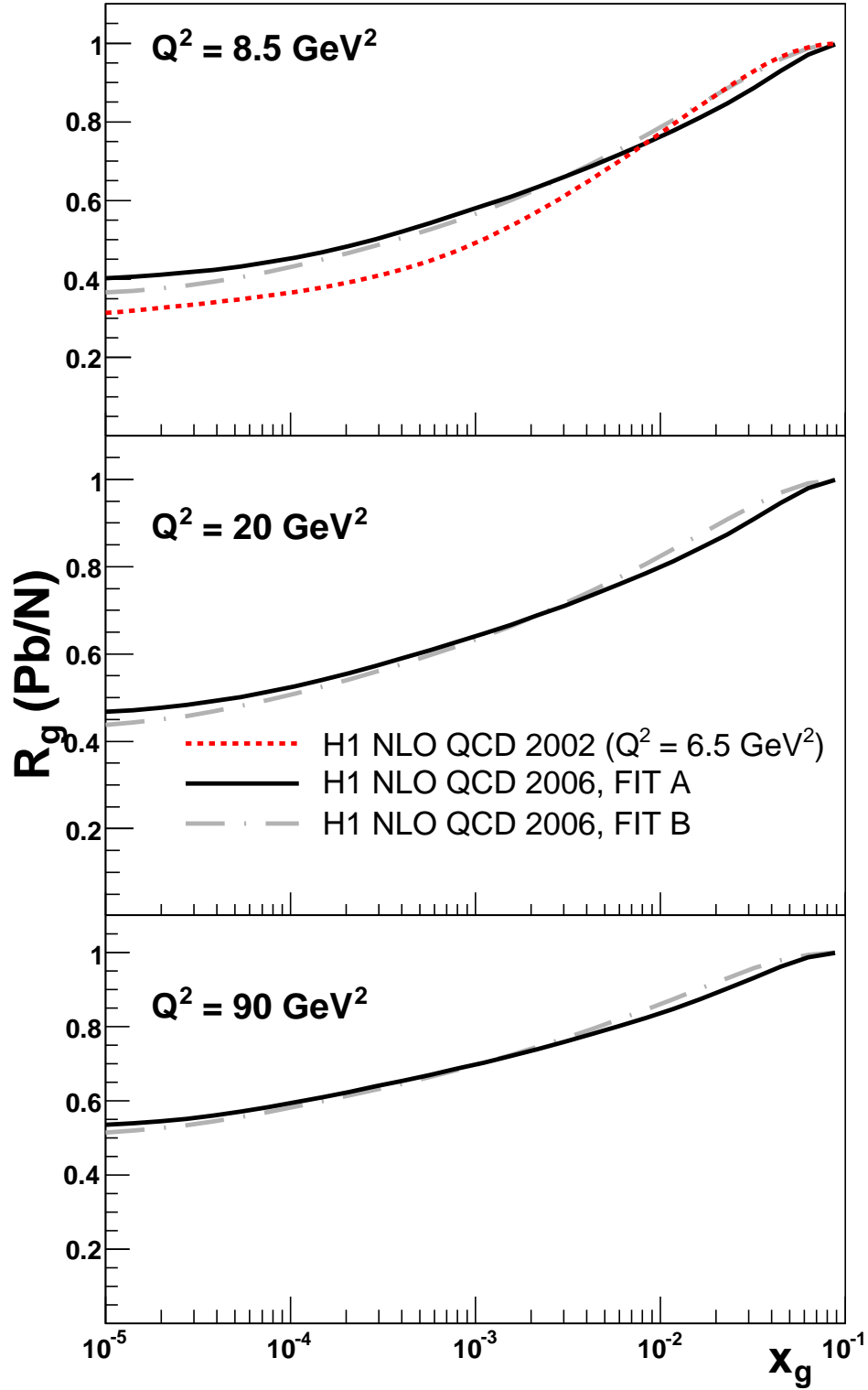


Figure 4: Gluon shadowing for Pb for different virtualities,  $Q^2$ .

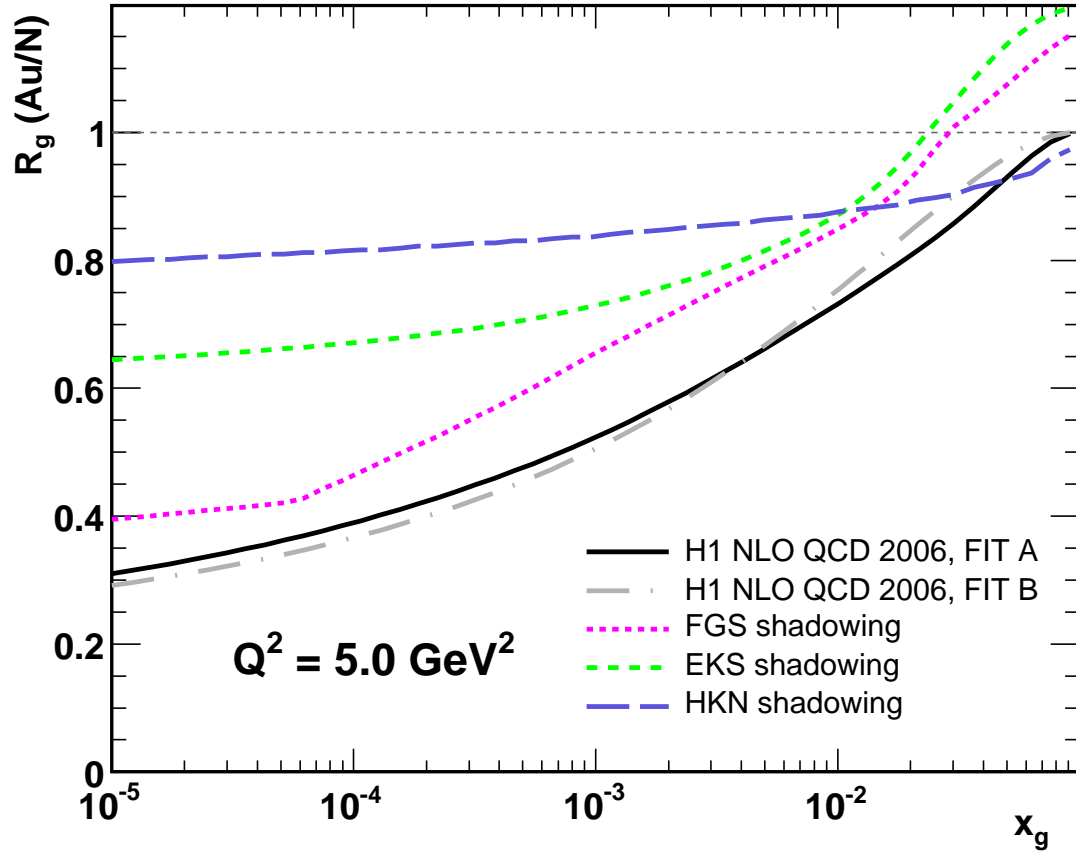


Figure 5: Comparison of the results of the Glauber-Gribov model with FGS model [24], EKS [33] and HKM [34] parameterizations.



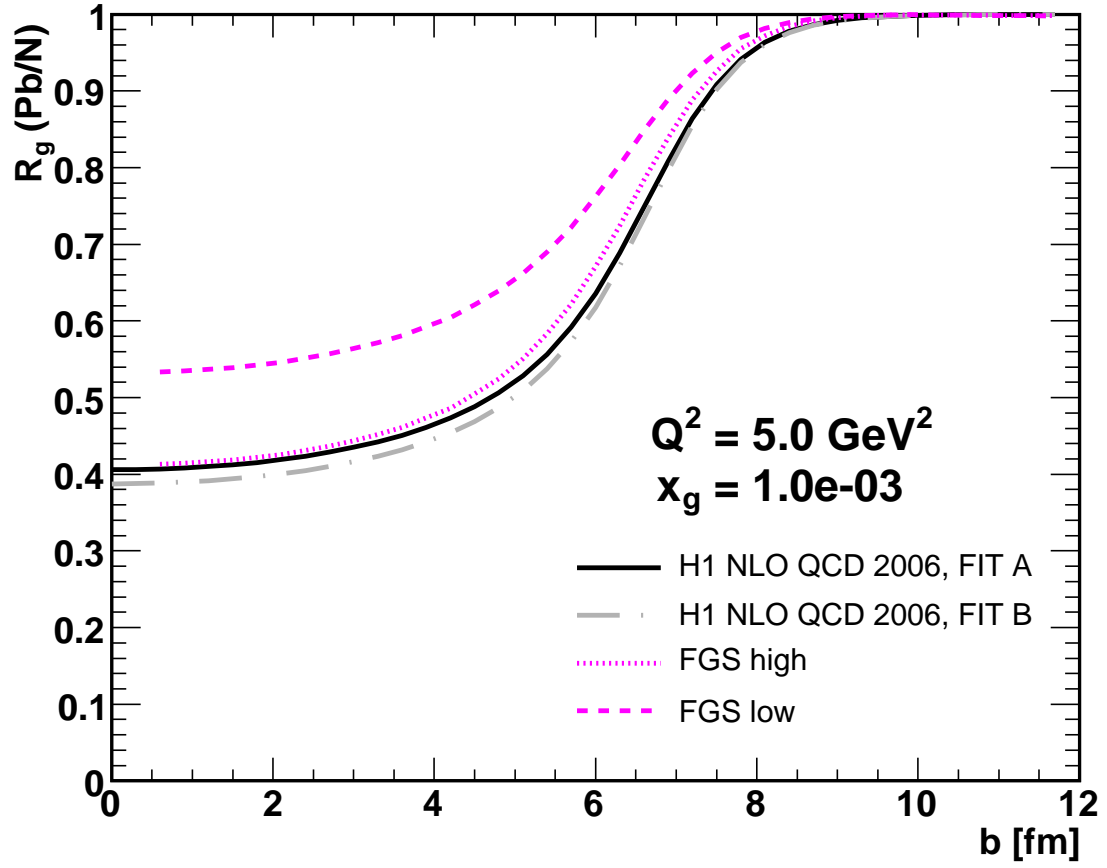


Figure 6: Impact parameter dependence of gluon shadowing in the Glauber-Gribov model, compared to the predictions of FGS [24].

**List of Tables**

1      Pomeron parameters from H1 Collaboration [25, 26, 29]. . . . . 19

$\alpha_{\mathbb{P}}(0)$ [FIT A]	1.118
$\alpha_{\mathbb{P}}(0)$ [FIT B]	1.111
$\alpha'_{\mathbb{P}}$	0.06 GeV <sup>-2</sup>
$B_0$	5.5 GeV <sup>-2</sup>
$\alpha_{\mathbb{P}}(0)$ [2002]	<i>1.173</i>
$\alpha'_{\mathbb{P}}$ [2002]	<i>0.26 GeV<sup>-2</sup></i>
$B_0$ [2002]	<i>4.6 GeV<sup>-2</sup></i>

Table 1: Pomeron parameters from H1 Collaboration [25, 26, 29].